Journal of Sound and Vibration (1996) **194**(1), 107–117

BIFURCATIONS AND CHAOS IN A RATE GYRO WITH HARMONIC EXCITATION

Z.-M. Ge and H.-H. Chen

Department of Mechanical Engineering, National Chiao Tung University, Hsinchu, Taiwan, Republic of China

(*Received* 8 *November* 1994, *and in final form* 16 *October* 1995)

1. INTRODUCTION

The stability of a single-axis rate gyro mounted on a space vehicle subject to a variety of motion has been analyzed by Singh [1] and Ge [2]. Further consideration is given here to the complex non-linear and chaotic motions of a rate gyro under harmonic excitation about the vehicle input axis. This is a non-linear system subjected to combined parametric and external excitations.

A number of studies on non-linear parametrically excited oxcillators over the past few decades have employed analytical approximation methods, in particular the averaging method [3] and the multiple scales method [4] on weakly non-linear systems, and the harmonic balance method (HBM) [5] for strongly non-linear systems. In this paper the latter method with the Floquet theorem [6] is used to analyze the stability of system attractors with strong non-linearities and parametric excitations. The HBM appears to handle strong non-linearities well, and provides accurate steady state solutions, but it requires an excessive amount of analytical work. Thus, the Galerkin technique with harmonic balancing with the fast Fourier transform algorithm [7] is used here to reduce the amount of computational work and obtain a higher order approximation. Finally, numerical techniques are used to detect the existence of symmetry-breaking bifurcation, subharmonic responses, period-doubling bifurcations, interior crisis and chaos.

A model of a single-rate gyro mounted on a space vehicle is considered, as shown in Figure 1. The gimbal rotates about the output axis X with rotational angle θ. Motion about this axis is resisted by the torisonal spring and damping torque defined by $K\theta$ and $C_d\dot{\theta}$, respectively. Using Lagrange's equation, one can derive the following differential equation for the output deflection angle θ of a rate gyro [2]:

$$(A + A_g)\ddot{\theta} + C_d\dot{\theta} + K\theta + Cn_R(\omega_Y \cos\theta + \omega_Z \sin\theta) + (A + B_g - C_g) \times (\omega_Y \cos\theta + \omega_Z \sin\theta)(\omega_Y \sin\theta - \omega_Z \cos\theta) = -(A + A_g)\dot{\omega}_X, \quad (1)$$

where

$$Cn_R = C(\dot{\psi} - \omega_Y \sin\theta + \omega_Z \cos\theta) = \text{constant}, \quad (2)$$

in which ω_X, ω_Y and ω_Z denote the angular velocity components of the platform along the output X-axis, the input Y-axis and the normal Z-axis, respectively. A, A and C, and A_g, B_g and C_g denote the moments of inertia of the rotor and gimbal, respectively.

Interest here is in the behavior of non-linear dynamical motion when the vehicle undergoes a steady rotation about the X-axis, and very small rotation with respect to the Z-axis, so that then $\dot{\omega}_X = 0$ and $\omega_Z \approx 0$. It is assumed that the rotation of the vehicle about the input Y-axis is harmonic: i.e., $\omega_Y = f \sin \omega_f t$; f and ω_f are the amplitude and the frequency of the input, respectively. For convenience, by using the parameters $\tau = \omega_n t$, $x = \theta$, $y = \dot{\theta}$, $\alpha = C_d/[2(A + A_g)\omega_n]$, $\beta = (A + B_g - C_g)f^2/[4(A + A_g)\omega_n^2]$, $\gamma =$

0022–460X/96/260107 + 11 $18.00/0

$Cn_R f/[(A + A_g)\omega_n^2]$, $\omega_n = \sqrt{K/(A + A_g)}$ and $\omega = \omega_f/\omega_n$, where the excitation frequency is close to twice the natural frequency, equation (1) can be changed into the dimensionless form

$$\ddot{x} + 2\alpha\dot{x} + x = -\beta \sin 2x + \beta \sin 2x \cos 2\omega\tau - \gamma \cos x \sin \omega\tau = g(x(\tau), \tau), \tag{3}$$

where $\beta = 2{\cdot}5 \times 10^{-5} f$, $\gamma = 0{\cdot}2f$ and $g(x(\tau), \tau)$ represents the non-linear forcing function; the other values of the gyro parameters [1] are given in the Appendix (I).

2. STABILITY ANALYSIS

When harmonic input is absent, equation (3) has a hyperbolic fixed point at the origin. With the addition of the harmonic input, the sink becomes a hyperbolic closed orbit and the effects of both external and parametric excitations gradually increase. Here, interest is in determining the stability limits of periodic orbits.

First, the approximate solution can be obtained by using the Galerkin technique with harmonic balancing. The steady state periodic solution can be represented as a Fourier series

$$x(\tau) \cong a_{0/q} + \sum_{k=1}^{n} \left(a_{k/q} \cos \frac{k\omega\tau}{q} - b_{k/q} \sin \frac{k\omega\tau}{q} \right), \tag{4}$$

where n is the order of the harmonic to be taken into account, and q is the order of the subharmonics. Similarly, the non-linear forcing function $g(x, \tau)$ can be expressed as

$$g(x, \tau) = c_{0/q} + \sum_{k=1}^{n} \left(c_{k/q} \cos \frac{k\omega\tau}{q} - d_{k/q} \sin \frac{k\omega\tau}{q} \right), \tag{5}$$

where $c_{0/q}$, $c_{k/q}$, and $d_{k/q}$ are given in the Appendix (II).

Substituting equations (4) and (5) into equation (3), and setting the coefficients of the constant, cos $(k\omega\tau/q)$, and sin $(k\omega\tau/q)$ terms to zero, yields the following non-linear $2n + 1$ algebraic equations:

$$C_0(v) = a_{0/q} + c_{0/q} = 0, \qquad C_k(v) = \left[1 - \left(\frac{k}{q}\omega \right)^2 \right] a_{k/q} - 2\alpha \left(\frac{k}{q}\omega \right) b_{k/q} + c_{k/q} = 0,$$

$$S_k(v) = 2\alpha \left(\frac{k}{q}\omega \right) a_{k/q} + \left[1 - \left(\frac{k}{q}\omega \right)^2 \right] b_{k/q} + d_{k/q} = 0, \qquad k = 1, 2, \ldots, n,$$

or

$$F(v) = Lv + w(v), \tag{6}$$

where $v = [a_{0/q}, \ldots, a_{n/q}, b_{n/q}]^T$, $w(v) = [c_{0/q}(v), \ldots, c_{n/q}(v), d_{n/q}(v)]^T$ and $F(v) = [C_0, \ldots, C_n, S_n]^T$. F is the corrective term which goes to zero when the approximate steady state is reached. One can solve the non-linear algebraic equations (6) to determine v by the Newton–Raphson iterative method. A neighbouring state is reached through a parameter incrementation

$$v = v_0 + \Delta v, \tag{7}$$

where $\Delta v = [\Delta a_{0/q}, \ldots, \Delta a_{n/q}, \Delta b_{n/q}]^{\mathrm{T}}$. By substituting equation (7) into equation (6), a $(2n+1)$ linearized incremental equation in terms of the correctors $\Delta a_{k/q}$ and $\Delta b_{k/q}$ is obtained from equation (6), namely

$$J\Delta v = F, \tag{8}$$

where $J = \partial F/\partial v = L + N_f$ is the first order derivative matrix and L is the linear part of the matrix J; the elements of the matrix $N_f = \partial w/\partial v|_{v=v_0}$ are given in the Appendix (II). Equation (8) defines an iterative solution algorithm for equation (6). After each iteration the v_0 are updated to $v_0 + \Delta v$. Convergence is indicated by the magnitude of F, since $F \to 0$ as $x_0 \to x^*$ (the steady state solution).

After this procedure, the approximate solution is determined by harmonic balancing and the Newton–Raphson iterative method.

To examine the local stability of the qT-periodic steady state solution $x_0(\tau)$, the perturbed solution is considered in the form

$$x(\tau) = x_0(\tau) + \xi(\tau). \tag{9}$$

Inserting equation (9) into equation (3), and ignoring the terms of higher order in ξ, one has a linear variational equation with periodic coefficients in the form

$$\ddot{\xi} + 2\alpha\dot{\xi} + \xi[1 + 2\beta \cos 2x_0(1 - \cos 2\omega\tau) - \gamma \sin x_0 \sin \omega\tau] = 0, \tag{10}$$

which can be arranged as

$$\ddot{\xi} + 2\alpha\dot{\xi} + \xi[1 + H(\tau)] = 0, \tag{11}$$

where

$$H(\tau) = \lambda_0 + \lambda_1(\tau) + \lambda_2(\tau), \qquad \lambda_1(\tau) = \lambda_1(\tau + qT), \qquad \lambda_2 = \lambda_2(\tau + qT/2),$$
$$T = 2\pi/\omega. \tag{12}$$

By applying Floquet theory [6], one obtains the particular solution of equation (10) in the form

$$\xi(\tau) = \exp[(\varepsilon - \alpha)\tau]\Phi(\tau), \tag{13}$$

where $(\varepsilon - \alpha)$ is the characteristic exponent which is positive in the instability region and $\Phi(\tau)$ is a periodic function. From equation (13) and the characteristics of a dynamical system and its solution, one can determine the behavior of the system under

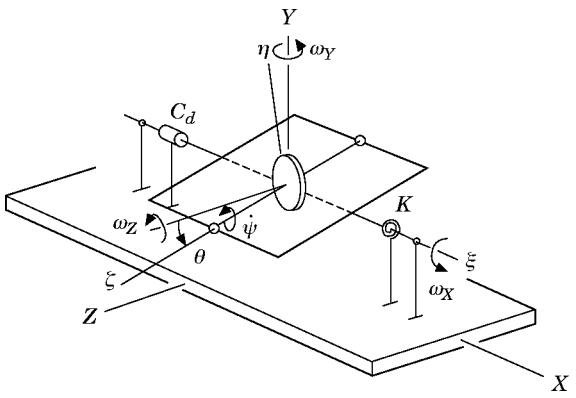

Figure 1. A rate gyro.

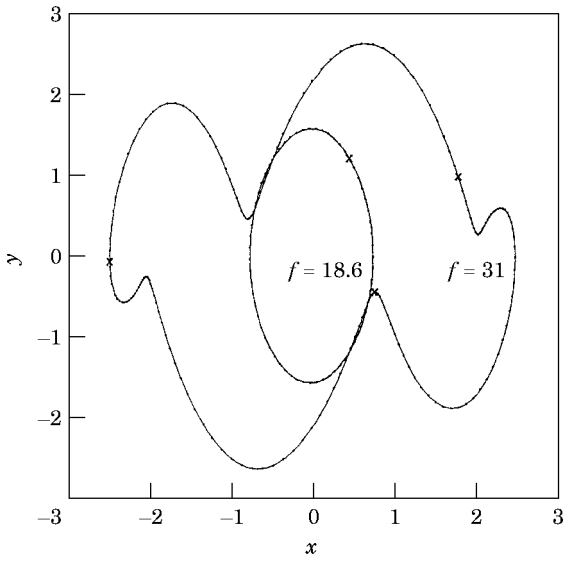

Figure 2. Two inversion-symmetric attractors as obtained by the Galerkin technique with harmonic balancing (· · · ·) and numerical integration (——) from equation (3).

symmetry-breaking and period-doubling bifurcations described by Szemplińska-Stupnicka [8].

Räty [9] has shown that oscillators with external excitation and antisymmetric non-linear terms possess inversion-symmetric attractors with odd periods: i.e., non-linear terms $F(-x) = -F(x)$, with the periods of the attractors $T_j = (2j-1)2\pi/\omega$. Similarily, the non-linear function $g(x, \tau)$ of a parametrically excited rate gyro suggests that these attractors are inversion-symmetric, or inversions of each other corresponding to the varying parameter f. If T_j is of odd period, the non-linear forcing function of this system satisfies the relation

$$g(x(\tau), \tau) = -g(-x(\tau), \tau + \tfrac{1}{2}T_j) = g(-\tilde{x}(\tau + \tfrac{1}{2}T_j),\ \tau), \tag{14}$$

where $x(\tau)$ and $\tilde{x}(\tau)$ are the steady state solutions of equation (3) related as follows: $x(\tau) = -\tilde{x}(\tau + \frac{1}{2}T_j)$ implies that the phase portraits of attractors $x(\tau)$ and $\tilde{x}(\tau)$ with odd periods coincide, i.e., $x(\tau) = \tilde{x}(\tau)$; the inversion-symmetric attractors are odd-period functions that coincide with the numerical simulation in period-T and period-$3T$ attractors, as shown in Figure 2. On the other hand, breaking of the inversion symmetry implies that a pair of attractors $x(\tau)$ and $\tilde{x}(\tau)$ are inversions of each other, as illustrated in Figure 5 of Section 3.

The symmetry-breaking instability boundary of the system can be studied as follows. For small system response, the non-linear terms $\sin x$ and $\cos x$ can be replaced by $(x - x^3/3!)$ and $(1 - x^2/2!)$, so that the governing equation becomes

$$\ddot{x} + 2\alpha\dot{x} + [x + \beta(2x - 4x^3/3)(1 - \cos 2\omega\tau)] = -\gamma(1 - x^2/2)\sin\omega\tau. \tag{15}$$

The approximate solution is assumed to be

$$x_0(\tau) = a_{1/q}\cos\frac{\omega\tau}{q} - b_{1/q}\sin\frac{\omega\tau}{q} + \sum_{i=3,5,\ldots} a_{i/q}\cos\frac{i\omega\tau}{q} - b_{i/q}\sin\frac{i\omega\tau}{q}, \tag{16}$$

where q is odd. From the previous procedure, one obtains the linear variational equation (15) in the form

$$\ddot{\xi} + 2\alpha\dot{\xi} + \xi[1 + \beta(2 - 4x_0^2)(1 \ - \cos 2\omega\tau) - \gamma x_0 \sin \omega\tau] = 0. \tag{17}$$

Because the solution x_0 is symmetric, the types of instability of a particular solution of equation (17) involve functions of period $T_q/2$,

$$\Phi(\tau) = \Phi\left(\tau + \frac{T_q}{2}\right) = r_0 + \sum_{j=1}^{n}\left(r_j \cos\frac{2j\omega\tau}{q} - s_j \sin\frac{2j\omega\tau}{q}\right), \tag{18}$$

where q is odd. To determine the period-T symmetry-breaking instability, one assumes the first approximate solution to be

$$\xi(\tau) = e^{(\varepsilon - \alpha)\tau}(r_0 + r_1 \cos 2\omega\tau - s_1 \sin 2\omega\tau), \tag{19}$$

which gives the following perturbed solution relation:

$$\tilde{x}(\tau + \tfrac{1}{2}T_1) + \xi(\tau + \tfrac{1}{2}T_1) = -x(\tau) + \xi(\tau), \qquad T_1 = T = 2\pi/\omega. \tag{20}$$

Therefore, the inversion symmetry has been broken. By inserting equation (19) into equation (17) and applying the harmonic balance method, the stability limit (where $\varepsilon - \alpha = 0$, can be obtained, as shown in Figure 3.

After symmetry-breaking bifurcation, period-doubling bifurcation begins. From the unsymmetric solution (4) and dynamical equation (3), one has $\lambda_1(\tau)$ of equation (12), which is an essential term to yield the period-doubling bifurcation. One may expect a particular solution of equation (11) in the same form as equation (13):

$$\Phi(\tau) = \Phi(\tau + 2qT) = \sum_{k=1,3}^{2n-1}\left(r_{cj/2q} \cos\frac{k\omega\tau}{2q} - r_{sj/2q} \sin\frac{k\omega\tau}{2q}\right). \tag{21}$$

When $\varepsilon - \alpha > 0$, this form of instability exists and a series of period-doubling bifurcations becomes possible. The stability limit can be obtained by substituting equation (21) into

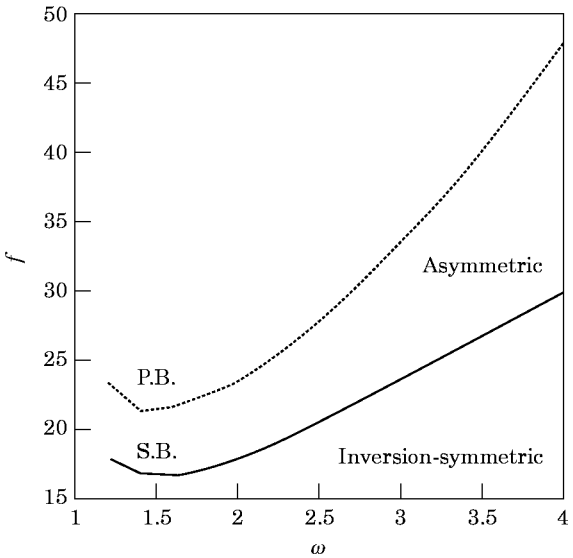

Figure 3. The bifurcation diagram for S.B. (symmetry-breaking bifurcation) and P.B. (period-doubling bifurcation), from equation (15).

equation (11), using the Galerkin technique and matching harmonic terms. Assuming $\varepsilon - \alpha = 0$, one has

$$C_k(\mu) = [1 - (k\omega/2q)^2]r_{ck/2q} - 2\alpha(k\omega/2q)r_{sk/2q} + s_{ck/2q} = 0,$$

$$S_k(\mu) = 2\alpha(k\omega/2q)r_{ck/2q} + [1 - (k\omega/2q)^2]r_{sk/2q} + s_{sk/2q} = 0, \qquad k = 1, 3, \ldots, 2n-1, \quad (22)$$

where $\mu = [r_{c1/2q}, \ldots, r_{ck/2q}, r_{sk/2q}]^T$ and $\sigma(\mu) = s_{c1/2q}(\mu), \ldots, s_{ck/2q}(\mu), s_{s/2q}(\mu)]^T$. The variation of equation (22) with respect to μ is

$$(R + S)\delta\mu = 0, \quad (23)$$

where

$$S = \frac{\partial\sigma}{\partial\mu}, \qquad R_{kj} = \mathbf{0}_{4\times 4} \quad k \neq j,$$

$$R_{kj} = \begin{bmatrix} 1 - \left(\dfrac{k\omega}{2q}\right)^2 & -2\alpha\left(\dfrac{k\omega}{2q}\right) \\ 2\alpha\left(\dfrac{k\omega}{2q}\right) & 1 - \left(\dfrac{k\omega}{2q}\right)^2 \end{bmatrix}_{4\times 4}, \quad k = j, \quad k = 1, 3, \ldots, \ 2n-1. \quad (24)$$

To determine the stability limit, one sets the Jacobian of equation (23) to zero, obtaining the characteristic equation $\Delta(\omega^2) = |(R + S)| = 0$. By considering the period-T solution ($q = 1$) with the first harmonic order ($k = 1$), and solving the characteristic equation, the stability curve is obtained in the parameter plane, as shown in Figure 3.

3. NUMERICAL SIMULATIONS AND DISCUSSIONS

As shown in Figure 2, the preceding analytical approximation method yields an attractor which is in good agreement with that obtained by numerical integration. It also reveals two types of bifurcations, as shown in Figure 3. Clearly distinct bifurcations and chaos are exposed in detail by various numerical simulations. The first type, which appears at point A in Figure 4 for $f \approx 18{\cdot}8$, is called symmetry-breaking bifurcation. The second type, which appears at point B in Figure 4 for $f \approx 24{\cdot}8$, is the period-doubling (flip) bifurcation. The third type, which appears at point E in Figure 4 for $f \approx 29{\cdot}1$, is the saddle-node (tangent) bifurcation. In this model, a sequence of bifurcations occurs and leads to chaos as the system parameter is varied.

The bifurcation diagram in Figure 4 shows the long-term values of the rotational angle, obtained by numerical integration, plotted against the dimensionless forcing amplitude f. Before point A (or G) in Figure 4, the orbit in the phase plane is an inversely symmetric cycle of period-T (or period-3T), as shown in Figure 2. At point A (or G) in Figure 4, a symmetry-breaking bifurcation occurs. After a bifurcation of this type, there occurs a cascade of period-doubling bifurcations from point B to point C (or point H-I) in Figure 4. When the parameter f approaches point C (or I), chaotic motion appears. Between point C and point D (or point I–J) in Figure 4, there exist two inverse chaotic attractors, as shown in Figure 5. As shown in Figure 4, when the parameter f passes beyond point D, conjunction of the two chaotic attractors creates a larger chaotic attractor similar to that in Figure 6. At point E in Figure 4, a stable period-3 orbit abruptly appears, but a chaotic attractor still exists (see Figure 6). The former is the saddle-node (tangent) bifurcation which also creates a period-unstable orbit. Upon passing point F in Figure 4, the chaotic attractor disappears, and the period-3 window is seen at the interval from point E to point J.

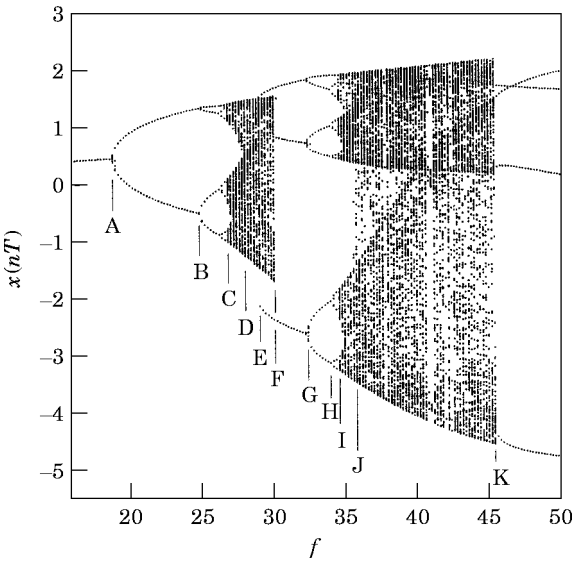

Figure 4. The bifurcation diagram for a rate gyro; steady state angular displacement $x(nT)$ versus the amplitude of excitation f, from equation (3).

Within the period-3 window from point I to point J in Figure 4, there are two inverse chaotic attractors, the mappings of which are confined to three narrow bands. After the period-3 window (just past point J in Figure 4), one sees a bifurcation from a chaotic attractor in three bands to a chaotic attractor in only one larger band. This bifurcation causes sudden changes in the size of the chaotic attractor which is called an "interior crisis" [10]. From point B to point C in Figure 4, a series of period-doubling routes to chaotic motion occur as system parameter is varied. The classic route to chaos via a cascade of period-doubling bifurcations can be described as the evolution of unsymmetric solutions due to the system possessing unsymmetric non-linear characteristics. From the averaged

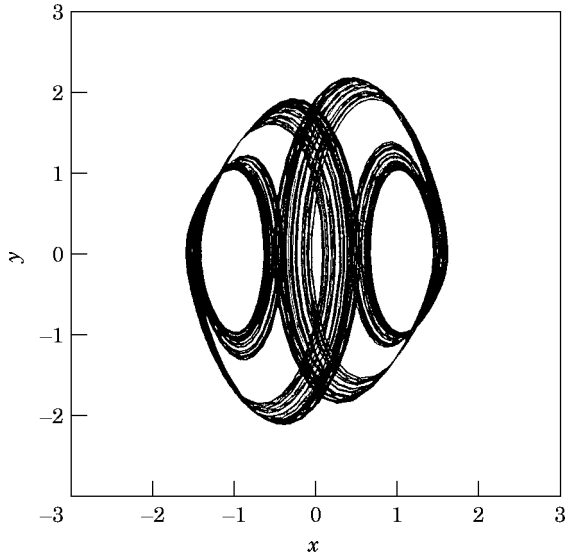

Figure 5. Two inverse chaotic attractors of the system equation (3) plotted in the phase plane for $f = 26{\cdot}8$.

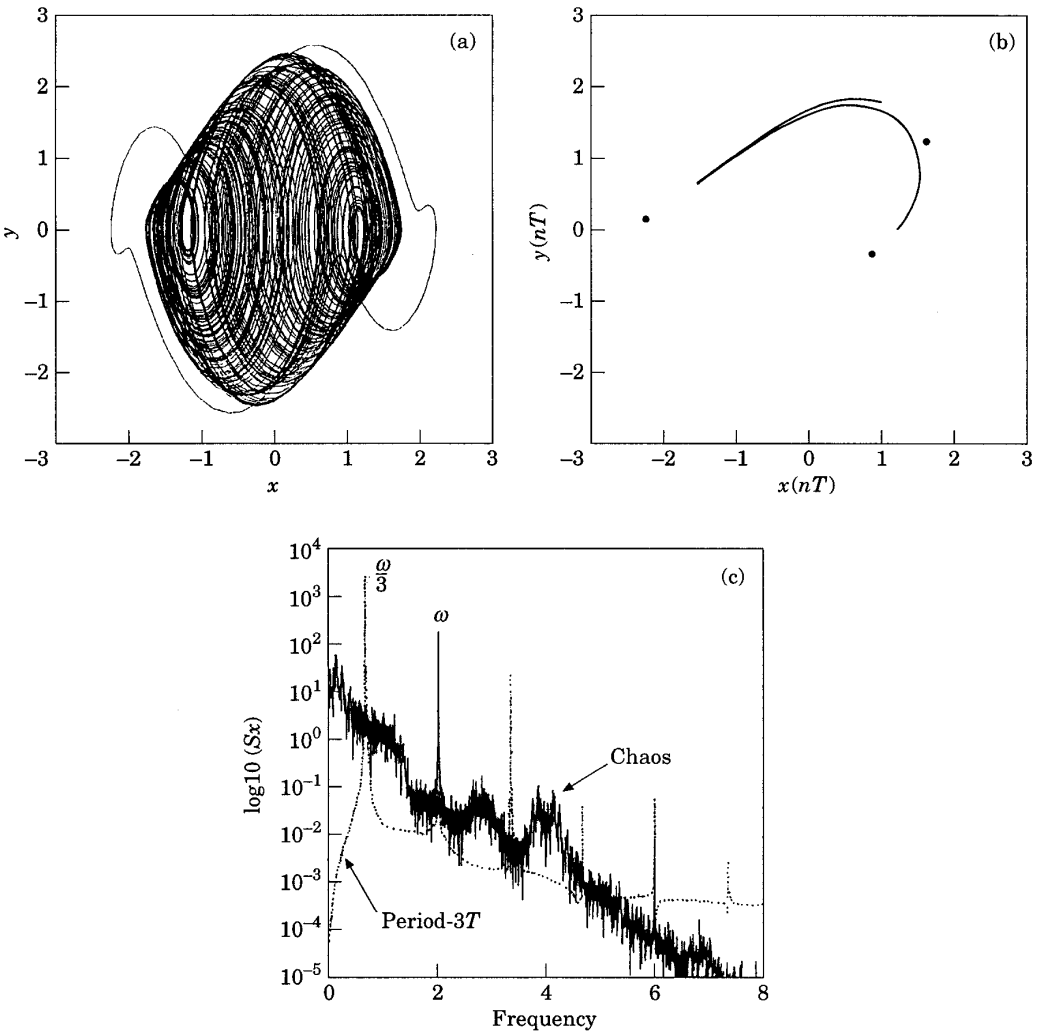

Figure 6. A large chaotic attractor coexisting with a period-3T limit cycle of the system (3) as shown by (a) a phase plane plot, (b) a Poincaré map, and (c) the average power spectrum, for $f = 29{\cdot}1$.

power spectrum $S_x(\omega)$, one also observes that a chaotic motion has a continuous broad spectrum, and shows random-like behavior (see Figure 6(c)).

In the period-3T windows, there also occurs a period-doubling cascade route to chaotic motion. As the system parameter f increases from point I to point J, a chaotic attractor in three bands gradually becomes larger until the parameter passes point J and the interior-crisis bifurcation occurs. When the parameter passes point K in Figure 4, the chaotic attractor disappears and two inverse attractors of period-2T occur. The values of A–K are shown in the Appendix (III).

In order to confirm the chaotic behavior, Lyapunov exponents have been calculated as $\lambda_1 = 0{\cdot}047$, $\lambda_2 = 0{\cdot}0$ and $\lambda_3 = -1{\cdot}431$ for $f = 26{\cdot}8$, as shown in Figure 7. The Lyapunov exponent calculation algorithm was proposed by Wolf *et al*. [11]. There exists a positive Lyapunov exponent which indicates the system to be chaotic. The sum of all the three Lyapunov exponents, $\lambda_1 + \lambda_2 + \lambda_3 = -1{\cdot}384$, is equivalent to the negative damping

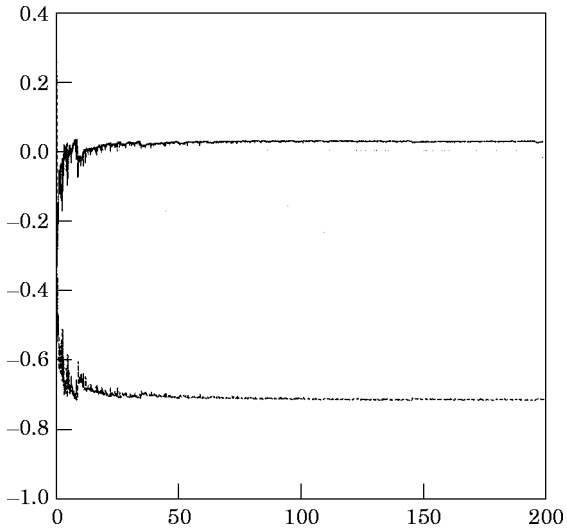

Figure 7. Lyapunov exponents for a rate gyro plotted as a function of the number of drive cycles are shown as (0·047, 0, −1·431) for $f = 26{\cdot}8$; the positive Lyapunov exponent shows that the system equation (3) is chaotic.

coefficient of the system. The Lyapunov dimension $d_L = 2{\cdot}0328$, for $f = 26{\cdot}8$, was also calculated by the relation described by Frederickson *et al*. [12],

$$d_L = j + \sum_{i=1}^{j} \lambda_i / |\lambda_{j+1}|, \tag{25}$$

where j is defined by the condition

$$\sum_{i=1}^{j} \lambda_i > 0 \qquad \text{and} \qquad \sum_{i=1}^{j+1} \lambda_i < 0. \tag{26}$$

4. CONCLUSIONS

The dynamics of a single-axis rate gyro subjected to parametric excitation have been investigated. By using the Galerkin technique with harmonic balancing, approximate periodic solutions and their stability have been analyzed. The modified harmonic balance method can reduce the amount of computation work and produce a good approximation. From the approximate analysis of local instability in variational equations of Hill's type, symmetry-breaking and period-doubling bifurcation behavior can be examined.

Results describing the behavior of a symmetry-breaking precursor of period-doubling bifurcations, and a cascade of period-doubling route to chaos in numerical simulations, have been shown through Poincaré maps, phase portraits, bifurcation diagrams, power spectral diagrams and Lyapunov-exponent diagrams. Additionally, interior crisis and chaotic attractors that coexist with periodic attractors were also found to occur in the system.

ACKNOWLEDGMENTS

The authors wish to thank the referees for their valuable and helpful comments on this paper. The authors are grateful to the National Science Council, Republic of China, for supporting this research under grant NSC 84-2212-E-009-021.

REFERENCES

1. S. N. Singh 1984 *IEEE Transactions on Aerospace and Electronic Systems* **AES-20**, 119–127. Gyro motion boundedness under uncertain vehicle spin and acceleration.
2. Z. M. Ge and C. J. Chen 1992 *AIAA Journal of Guidance, Control, and Dynamics* **15**, 1034–1036. Stability of a rate gyro.
3. K. Yagasaki, M. Sakata and K. Kimura 1990 *Transactions of the American Society of Mechanical Engineers, Journal of Applied Mechanics* **57**, 209–217. Dynamics of a weakly nonlinear system subjected to combined parametric and external excitation.
4. N. E. Sanchez and A. H. Nayfeh 1990 *International Journal of Non-linear Mechanics* **25**, 163–176. Prediction of bifurcations in a parametrically excited duffing oscillator.
5. W. Szemplińska-Stupnicka, R. H. Plaut and J.-C. Hsieh 1989 *Transactions of the American Society of Mechanical Engineers, Journal of Applied Mechanics* **56**, 947–952. Period doubling and chaos in unsymmetric structures under parametric excitation.
6. G. Ioos and D. D. Joseph 1981 *Elementary Stability and Bifurcation Theory*. New York, Springer-Verlag.
7. F. H. Ling and X. X. Wu 1987 *International Journal of Non-linear Mechanics* **22**, 89–98. Fast Galerkin method and its application to determine periodic solutions of non-linear oscillators.
8. W. Szemplińska-Stupnicka 1987 *Journal of Sound and Vibration* **113**, 155–172. Secondary resonances and approximate models of routes to chaotic motions in non-linear oscillations.
9. R. Räty, J. Von Boehm and H. M. Isomäki 1984 *Physics Letters* **103A**, 289–292. Absence of inversion-symmetric limit cycles of even periods and the chaotic motion of Duffing's oscillator.
10. C. Grebogi, E. Ott and J. A. Yorke 1982 *Physical Review Letters* **48**, 1507–1510. Chaotic attractors in crisis.
11. A. Wolf, J. B. Swift, H. L. Swinney and J. A. Vastano 1985 *Physica* **16D**, 285–317. Determining Lyapunov exponents from a time series.
12. P. Frederickson, J. L. Kaplan, E. D. Yorke and J. A. Yorke 1983 *Journal of Differential Equations* **49**, 185–207. The Lyapunov dimension of strange attractors.

APPENDIX

I. The values of the gyro parameters are as follows:

$$\frac{C_d}{(A+A_g)} = 140 \text{ rad}^{-1}\text{ s}^{-1}, \qquad \frac{K}{(A+A_g)} = 10^4 \text{ rad}^{-1}\text{ s}^{-2}, \qquad \frac{Cn_R}{(A+A_g)} = 2000 \text{ s}^{-1},$$

$$\frac{(A+B_g-C_g)}{(A+A_g)} = 1,$$

$$\omega_n = 100 \text{ rad s}^{-1}, \qquad \omega = \omega_f/\omega_n = 2, \qquad \alpha = 0{\cdot}7, \qquad \beta = 2{\cdot}5 \times 10^{-5} f^2, \qquad \gamma = 0{\cdot}2f.$$

II. The coefficients of the Fourier transform of the non-linear forcing function $g(x, \tau)$ are given by

$$c_{0/q} = \frac{1}{T_q}\int_0^{T_q} g(x,\tau)\,\mathrm{d}\tau, \qquad c_{p/q} = \frac{2}{T_q}\int_0^{T_q} g(x,\tau)\cos\frac{p\omega\tau}{q}\,\mathrm{d}\tau,$$

$$d_{p/q} = \frac{2}{T_q}\int_0^{T_q} g(x,\tau)\sin\frac{p\omega\tau}{q}\,\mathrm{d}\tau. \tag{II1}$$

Let $T_q = N\,\Delta\tau$, $\mathrm{d}\tau = \Delta\tau$, $\tau = r\,\Delta\tau$, $\Delta\tau \to 0$; equation (II1) then becomes

$$c_{0/q} = \frac{1}{N}\sum_{r=0}^{N-1} g(x,r), \qquad c_{p/q} = \frac{2}{N}\sum_{r=0}^{N-1} g(x,r)\cos\frac{2\pi pr}{N}, \qquad d_{p/q} = \frac{2}{N}\sum_{r=0}^{N-1} g(x,r)\sin\frac{2\pi pr}{N}. \tag{II2}$$

The Jacobian matrix is

$$N_f = \partial w/\partial v|_{v=v_0} = \partial[c_{0/q}, \ldots, c_{p/q}, d_{p/q}]/\partial[a_{0/q}, \ldots, a_{k/q}, b_{k/q}]|_{v=v_0}. \tag{II3}$$

The elements of the Jacobian matrix N_f are expressed as follows:

$$\frac{\partial c_{0/q}}{\partial a_{0/q}} = \frac{1}{N}\sum_{r=0}^{N-1} g', \qquad \frac{\partial c_{0/q}}{\partial a_{k/q}} = \frac{1}{N}\sum_{r=0}^{N-1} g' \cos\frac{2\pi kr}{N}, \qquad \frac{\partial c_{0/q}}{\partial b_{k/q}} = -\frac{1}{N}\sum_{r=0}^{N-1} g' \sin\frac{2\pi kr}{N},$$

$$\frac{\partial c_{p/q}}{\partial a_{k/q}} = \frac{2}{N}\sum_{r=0}^{N-1} g' \cos\frac{2\pi pr}{N}\cos\frac{2\pi kr}{N}, \qquad \frac{\partial c_{p/q}}{\partial b_{k/q}} = -\frac{2}{N}\sum_{r=0}^{N-1} g' \cos\frac{2\pi pr}{N}\sin\frac{2\pi kr}{N},$$

$$\frac{\partial d_{p/q}}{\partial a_{k/q}} = -\frac{2}{N}\sum_{r=0}^{N-1} g' \sin\frac{2\pi pr}{N}\cos\frac{2\pi kr}{N}, \qquad \frac{\partial d_{p/q}}{\partial b_{k/q}} = \frac{2}{N}\sum_{r=0}^{N-1} g' \sin\frac{2\pi pr}{N}\sin\frac{2\pi kr}{N},$$

$$p, k = 1, 2, \ldots, n\ . \tag{II4}$$

Here N is the number of samples in the FFT; $g' = \partial g(x, r)/\partial x|_{x=x_0}$ can be expressed as

$$g' = -2\beta \cos 2x_0\{1 - \cos(4\pi qr/N)\} + \gamma \sin x_0 \sin(2\pi qr/N), \tag{II5}$$

where

$$x_0 = \left[a_{0/q} + \sum_{k=1}^{n}\left(a_{k/q}\cos\frac{2\pi kr}{N} - b_{k/q}\sin\frac{2\pi kr}{N}\right)\right]_{v=v_0}. \tag{II6}$$

III. The critical values (points A–K) shown in Figure 4 are the following:

A $\approx$ 18·8, B $\approx$ 24·8, C $\approx$ 26·8, D $\approx$ 28, E $\approx$ 29·1, F $\approx$ 30·05,
G $\approx$ 32·4, H $\approx$ 34·1, I $\approx$ 34·6, J $\approx$ 35·8, K $\approx$ 45·4.